Danish Meteorological Institute
Ministry for Energy, Utilities and Climate

DMI Report 16-23

Sensitivity study of visibility forecasts based on modifications to the visibility scheme in the nowcasting model at DMI

Niels Woetmann Nielsen, Bjarne Amstrup and Kasper Hintz

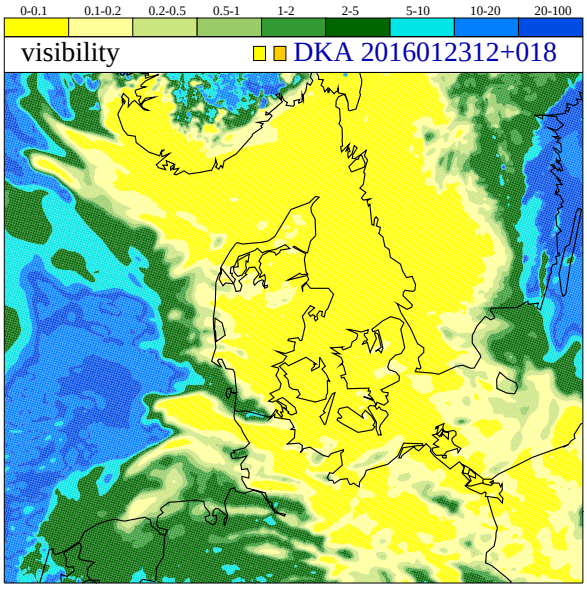

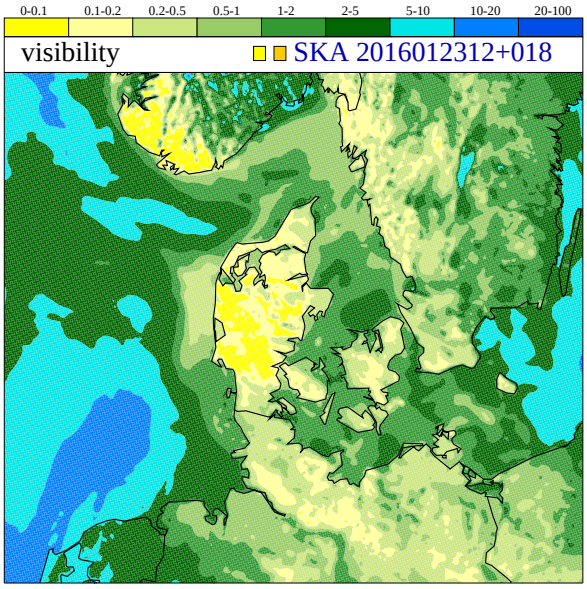

Danish Meteorological Institute
DMI Report 16-23

Colophone Serial title:
DMI Report 16-23

Title:
Sensitivity study of visibility forecasts based on
modifications to the visibility scheme
in the nowcasting model at DMI

Subtitle:

Authors:
Niels Woetmann Nielsen, Bjarne Amstrup and Kasper Hintz

Other Contributers:

Responsible Institution:
Danish Meteorological Institute

Language:
English

Keywords:
visibility, fog, nowcasting model

Url:
www.dmi.dk/laer-om/dmi-publikationer/2013/16-23

ISSN:
2445-9127

Version:

Link til hjemmeside:
www.dmi.dk/laer-om/dmi-publikationer/2013

1 Introduction

At the Danish Meteorological Institute (DMI) a diagnostic calculation of visibility at screen level (2m above ground), Vis2m, has been implemented in the DMI nowcasting model based on HIRLAM (High Resolution Limited Area Model). The scheme has been in operational use since February 2001. The predicted Vis2m is currently verified against visibility reports from about 30 Danish SYNOP stations. A simple interpolation from nearest model grid point to the observation location is applied. By this verification procedure high scores of Vis2m can only be expected if both the spatial pattern and time evolution of visibility is accurately predicted. Verification results have been available since February 2001. Generally, the verification results are found to be sensitive to model-system changes, in particular to changes in its surface scheme. Verification results show that the scheme has a clear tendency to predict too many low visibility (Vis2m < 1000 m) cases and too few high visibility (Vis2m > 20 km) cases. In the present report several modifications to the operational visibility scheme, OPR, and their impact on visibility scores are described. Section 2 briefly presents arguments for the development of a partly statistically based visibility scheme for operational use. Different types of fog are discussed in Section 3. This section also contains the applied definition of visibility. Section 4 gives a brief description of the operational diagnostic visibility scheme, OPR. More details about this scheme are given in Petersen and Nielsen, 2000. Section 5 contains a description of different experiments, where each experiment contains one or more modifications to OPR. Verification results for these experiments are discussed in Section 6, and all of them use the same wind velocity dependent aerosol contribution to visibility. A new population dependent aerosol contribution is introduced in Section 7, and a number of further experiments including the population dependent aerosol contribution are presented in Section 8 followed by a discussion of verification results from these experiments in Section 9. Finally Section 10 contains a summary and an outlook.

2 A statistically based visibility scheme

To some extent the diagnostic calculation of visibility is based on a statistical analysis of SYNOP reports from about 30 Danish stations covering a continuous period of 2 years (Figure 1 in Petersen and Nielsen, 2000). For this reason the derived formula is likely to be optimized for the prevailing meteorological conditions in Denmark. It may be less optimized in for example mountain regions and more generally in a different climate.

The visibility of air mainly depends on the content of aerosols, cloud water and precipitation particles. In accurate calculations the dependency of the visibility on the droplet size distribution in a fixed amount of cloud water must be considered. As a further complexity, the droplet size distribution depends on the number and properties of aerosols acting as condensation nuclei.

In the DMI-HIRLAM model aerosol properties are not accounted for in the visibility computation. The direct effect of aerosols on visibility is therefore calculated in a very simple way. Its indirect effect on visibility through its impact on the cloud water droplet size distribution has not been taken into account.

Cloud water (cw) is a prognostic variable in DMI-HIRLAM, calculated at each model level. At the surface cw is set to zero. In principle cw at the lowest model level could be used to diagnose the effect of cw on Vis2m. However, two difficulties are encountered. Firstly, there is no theoretically well-based method available which can be used to calculate cw at 2 m height from the models vertical cw profile. Secondly, fog (and in particular radiation fog) often is present in a thin layer within the lowest model layer, and this kind of fog may therefore not be seen/detected by the model.

For this reason the present stage of development does not make use of the predicted cw. Instead a pseudo cloud water (pcw) at 2 m height is calculated from model information about solar zenith angle, cloud cover and wind velocity, together with temperature and specific humidity at three levels: surface, screen level and lowest model level. Details about the calculation of pcw is given in Section 4.

The impact of precipitation on Vis2m has been taken into account by making use of the model-prediction of rain and snow intensity.

There is reason to believe that running the same model version with higher horizontal and not least vertical resolution, combined with a more detailed and accurate description of surface parameters (first of all soil moisture) would improve on the prediction scores for fog. Despite of this expectation the diagnostic formula for Vis2m in operational use must be considered as preliminary. More than 15 years of operational experience has shown that the scheme in its present form has a relatively high false alarm rate for low visibility ($< 1000\,\mathrm{m}$) and tends to underestimate good visibility ($> 20\,\mathrm{km}$).

The work presented here consists of modifications to the operational visibility scheme with the goal to improve the visibility scores, and in particular the scores for low visibility. This is not an easy task due to high sensitivity of low visibility to small changes in temperature and specific humidity, which means that small errors in the prediction of these parameters can lead to erroneous visibility predictions even if the visibility scheme is "perfect". Furthermore, the applied model does not consider aerosols. The visibility is influenced by the type and abundance of aerosols. The lack of aerosols in the model therefore contributes to errors in the predicted visibility. One of the modifications deals with a method to improve on the aerosol effect on visibility. This method is described in subsection 7.2.

3 Fog and visibility

The visibility in the atmosphere is reduced mainly because of scattering of light. The scattering occurs on air molecules, aerosols (including dust, smoke and salt particles), cloud droplets and hydrometeors. It is a common experience that the visibility drops dramatically from cloud free air to clouds. At the surface the latter significantly changes the visibility if fog forms locally or is advected from a nearby source.

3.1 Fog

Fog (cloudy air) forms in the atmosphere if its state changes from q, T, p to q', T', p' such that $q' = qs(T', p')$ where $qs(T', p')$ is the saturation specific humidity at temperature T' and pressure p'. The effect of changing pressure is usually small. Therefore moistening and cooling are the processes that most frequently transforms the atmospheric state to saturation. Also drying and cooling can lead to saturation if the cooling dominates, and likewise moistening and warming can generate fog if the moistening dominates. In an unsaturated environment the moisture of the air changes by the following processes: Turbulent mixing of air masses with different moisture content, turbulent and molecular transport of moisture to or from the underlying surface, and evaporation from precipitation falling through the air. If the air is saturated or supersaturated condensation takes place at a rate that keeps the atmospheric state near saturation. The visibility of the air decreases with increasing amount of condensate suspended in the air (equation (4)). Heating and cooling of the atmospheric state can occur as the result of: turbulent mixing of air masses with different temperature, turbulent and molecular sensible heat flux to or from the underlying surface, radiative cooling at the surface and radiative flux divergence in the atmosphere.

Fog has been classified in terms of the processes listed above. The main classes are

- Advection fog
- Frontal fog
- Radiation fog

Turbulent mixing dominates in advection fog. The latter typical forms when cold and moist air flows over warmer water or when warm and moist air flows over a cold water (or a cold and wet land) surface. If the horizontal surface pressure gradient is week the turbulent mixing may die out and in absence of radiative cooling prevent formation of fog in the latter case.

Frontal fog typically forms as a result of moistening of the subfrontal cool and unsaturated air by evaporation from hydro-meteors falling from the frontal clouds aloft.

Radiative cooling at the surface and in the air (in case of radiative flux divergence) dominates in radiation fog. Radiation fog may form initially above the surface as the result of cooling due to radiative flux divergence. Often, and in particular if the surface is wet, radiation fog first forms at the surface and grows in depth if the radiative cooling continues. After the initial formation of fog at the surface the maximum in radiative cooling becomes displaced from the surface to the top of the fog layer.

Vegetation has a significantly lower heat capacity than bare soil. Consequently vegetation cools faster than bare soil and saturation first occurs at the vegetation. In this phase turbulence and molecular interactions transport moisture from the air and the wet soil to the vegetation, where it condenses as dew or rime. The radiative cooling may continue without formation of fog until the air at the surface becomes saturated. If the air and soil are sufficiently dry radiative cooling at the surface may not persist long enough to saturate the air. The latter situation is not uncommon over land in summer in middle and high latitudes. In these conditions it is often observed that radiation fog only forms locally over patches of wet land and in particular in combination with a local minimum in terrain height. More generally, radiation fog typically forms over land in clear nights with calm winds. A review of theoretical work on fog is presented in Cotton and Anthes, 1989.

3.2 Visibility

Visibility is a measurement of how far away an object can be seen. This depends on the luminance, I, of the object and the physical state of the atmosphere. The rate of change of the luminance with horizontal distance x from the object is

$$\frac{dI}{dx} = -\beta(x)I(x), \tag{1}$$

where β is the extinction coefficient, which includes absorption and scattering of light. Integration over the horizontal distance from the object ($x = 0$) to the observer ($x = x_{\mathrm{obs}}$) gives

$$I(x_{\mathrm{obs}}) = I(0)\exp\left(-\int_0^{x_{\mathrm{obs}}}\beta(x)dx\right) = I_0\exp\left(-\overline{\beta}x_{\mathrm{obs}}\right), \tag{2}$$

where $\overline{\beta}$ is a mean value of β. From (2) follows

$$x_{\mathrm{obs}} = -\frac{1}{\overline{\beta}}\ln\frac{I}{I_0}. \tag{3}$$

Table 1: Extinction coefficients as proposed by Kunkel, 1984.

Cloud liquid water	$\beta = 144.7\, C^{0.88}$
Rain	$\beta = 1.100\, C^{0.75}$
Cloud ice	$\beta = 163.9\, C^{1.00}$
Snow	$\beta = 10.40\, C^{0.78}$

An object is considered to be invisible if $I/I_0 \leq 0.02$, which means that the visibility (in km) becomes

$$\vartheta = -\frac{1}{\beta}\ln(0.02). \tag{4}$$

The extinction coefficients for various hydro-meteors have been estimated by Kunkel,1984. C in this Table is the density of hydro-meteors in $\mathrm{g\,m^{-3}}$.

4 The diagnostic visibility algorithms

OPR is the visibility scheme in operational use in DMI-HIRLAM (as of March 2016). The scheme is described briefly in this section. It is assumed that contributions to visibility can be written as the sum

$$\sigma_{\mathrm{tot}} = \sigma_{\mathrm{bg}} + \sigma_{as} + \sigma_{\mathrm{eff}}, \tag{5}$$

where σ_{bg} is a background (clean air) contribution, σ_{as} an aerosol (polluted air) contribution and σ_{eff} a combined contribution from cloud water and precipitation. The background and aerosol contributions (σ_{bg} and σ_{as}, respectively) are specified in $\mathrm{g\,m^{-3}}$. This is also the case for σ_{eff}, but the calculation of this quantity is more complicated. The visibility (at 2 m height) in m is obtained from

$$\vartheta = d \cdot \sigma_{\mathrm{tot}}^{-0.88}, \tag{6}$$

where $d = -1000\ \ln(0.02)/144.7 = 27.0$ and 144.7 is the constant in the extinction coefficient for cloud water (Table 1). Note that the factor 1000 in d converts the visibility from km to m.

In the operational visibility code, OPR, $\sigma_{\mathrm{bg}} = 1.8 \cdot 10^{-4}\,\mathrm{g\,m^{-3}}$, corresponding to a background visibility of about 53 km. The aerosol contribution is parameterized simply as

$$\sigma_{as} = \sigma_0 \frac{v}{2+v}\sin(dd - 90), \tag{7}$$

where v is wind speed at 10 m height, dd wind direction and $\sigma_0 = 0.8 \cdot 10^{-4}\,\mathrm{g\,m^{-3}}$. σ_{eff} is calculated as

$$\sigma_{\mathrm{eff}} = \sigma_r + \sigma_s + \sigma_{pcw} \cdot \exp(-2.8\sqrt{\dot{r} + \dot{s}}). \tag{8}$$

In (8) σ_{pcw} is the contribution from pseudo cloud water (pcw) at screen level and $\dot{r}$ and $\dot{s}$ are the rain and snow intensity, respectively. Further $\sigma_r = 0.04\,\dot{r}^{4/9}$ and $\sigma_s = 1.90\,\dot{s}^{2/3}$ (for more details see Petersen and Nielsen, 2000). With increasing precipitation intensity the amount of pcw decreases because precipitation hydrometeors "collect" cw on their surfaces. This process is parameterized by the last term in (8). For reasons explained in the Section 2 pcw replaces cloud water, cw, at the lowest model level. pcw is to some extent using results from statistical analyses performed for a two year

period as described in Petersen and Nielsen, 2000. The proposed algorithm for pcw in the latter report is

$$\sigma_{pcw} = f_{sd} \cdot f_w. \tag{9}$$

In (9)

$$f_{sd} = 0.25 \left(1 + \frac{N}{8}\right) \left(1 + \frac{\widehat{dt}}{1 + \widehat{dt}}\right), \tag{10}$$

is a function of dew point depression $dpd = T - T_d$ and a crude imitation of the effect of static stability through the cloud cover N in octals and zenith angle z, appearing in

$$\widehat{dt} = \frac{(dt + 1 - r_n + (1 - r_2)(1 - \frac{q_2^*}{q_n^*}))}{(1 - c_3 \cdot \cos z)}. \tag{11}$$

T_d is the dew point temperature (in K) and dt a slightly modified dpd given by

$$dt = (1 - fl)dt_{\text{sea}} + fl \cdot dt_{\text{land}}, \tag{12}$$

where $dt_{\text{sea}} = dpdn + 0.1$, fl is fraction of land and

$$dt_{\text{land}} = dpd2 + c_0. \tag{13}$$

$dpd2$ and $dpdn$ are the dew point depressions at 2 m height and lowest model level, respectively. Further, r_2 and r_n are the relative humidity and q_2^* and q_n^* the saturation specific humidity at 2 m height and the lowest model level, respectively. The constants have the values $c_0 = 0.02$ and $c_3 = 1$. The former constant prevents the visibility from becoming zero if both wind speed and dpd are zero. The function f_w depends on both wind speed, v, and dpd. It has the form

$$f_w = \exp(-\alpha(f_{v1}\widehat{dt} + f_{v2})), \tag{14}$$

where $f_{v1} = \delta \cdot x(x - x_0) + c_2$ and $f_{v2} = \delta c_1 x^2 (x - x_0)$. Here $x = (2v + 1)^{1/3}$, $x_0 = (2v_0 + 1)^{1/3}$ and $\delta = \delta_0(1 + \delta_0 x^2)^{-1}$. The constants have the values $v_0 = 3.5\,\mathrm{m\,s^{-1}}$, $\delta_0 = 2x_0^{-2}$, $c_1 = 0.2$ and $_2 = 1$. The function f_{v1} represents the correlation between the frequency of low visibility and the product of dpd and v found in the observations (Petersen and Nielsen, 2000). The factor α in (14) is

$$\alpha = \alpha_0 - \frac{\widehat{dt} f_a}{1 + f_a \cdot f_b \widehat{dt}} \tag{15}$$

which determines how fast f_w responds to changes in $\widehat{dt}(dpd)$. In (15) $f_a = \alpha_0(1 + 2\alpha_0\widehat{dt})$ and $f_b = \hat{\varepsilon} + 1/\alpha_0$ with $\hat{\varepsilon} = \varepsilon_a - \widehat{dt}(\varepsilon_b/(1 + \widehat{dt}\varepsilon_b/\varepsilon_a))$, $\alpha_0 = 4$, $\varepsilon_a = 0.15$ and $\varepsilon_b = 0.20$.

5 Modifications to the operational visibility scheme: Part 1

The modifications can be grouped into three parts. One part modifies the background clean air) visibility, a second part modifies σ_{pcw}, that is how this parameter is calculated from atmospheric state variables, and a third part considers the aerosol contribution to visibility. In the present section only modifications of σ_{bg} and σ_{pcw} are considered.

5.1 Experiment R0V

Experiment R0V contains a few changes as compared to OPR (with names r0V, r0S, r0W, r0P, r0N in Figure 1). Firstly, the background visibility σ_0 has been set to zero with the condition that $\sigma_{\rm tot}$ must not become less than $1.5 \cdot 10^{-4}\,\mathrm{g\,m^{-3}}$, corresponding to a visibility that must not exceed 63 km. Secondly, the indirect static stability dependence in (10) and (11) has been replaced by an explicit dependence on a surface layer bulk Richardson number, Ri_b, defined by

$$Ri_b = \frac{g}{\sqrt{\theta_{vn}\theta_{vs}}} \frac{(\theta_{vn} - \theta_{vs}) z_n}{{u_n}^2 + {v_n}^2}. \tag{16}$$

In (16) θ_v is the virtual potential temperature and subscripts n and s mean lowest model level and surface, respectively. In (12) $dt_{\rm land}$ is replaced by

$$dt_{\rm land} = 0.5(dt2 + dtn) + 0.01\left(1 - \frac{Ri_b}{1 + |Ri_b|}\right) \tag{17}$$

and dt is replaced by

$$dt = ((1 - fl)dt_{\rm sea} + fl \cdot dt_{\rm land})\left(1 + \frac{cw_n}{cw_0}\right)^{-1}, \tag{18}$$

where cw_n is cloud water at the lowest model level and $cw_0 = 1 \cdot 10^{-5}\mathrm{g\,m^{-3}}$. The last term in (18) means that presence of cloud water at the lowest model level decreases visibility at 2 m height by decreasing dt. $\widehat{dt}$ given by (11) now reads

$$\widehat{dt} = (sta \cdot f_p + (1 - sta) f_m)\left(dt + 1 - r_n + (1 - r_2)(1 - \frac{{q_2}^*}{{q_n}^*})\right). \tag{19}$$

In the latter equation $sta = 1$ if $Ri_b \geq 0$ and $sta = 0$ if $Ri_b < 0$. The stability functions are specified as

$$f_p = 0.5(c_n + c_a(1 + 0.5 \cdot Ri_b)^{-2}) \tag{20}$$

and

$$f_m = 0.5(c_n + c_a(1 - 0.5 \cdot Ri_b)), \tag{21}$$

with $c_n = 2$ and $c_a = 4$, such that $\widehat{dt}$ is a decreasing function of Ri_b. In neutral stratification ($Ri_b = 0$) $f_p = f_m = 0.5(c_n + c_a)$. Since the stability functions to some extent takes into account the effect of wind speed on visibility the functions f_{v1} and f_{v2} in (14) are set to zero, implying $f_w = \exp(-\alpha)$. In (10) f_{sd} is replaced by $f_{sd} = 1 + \frac{\widehat{dt}}{1+\widehat{dt}}$ and in (6) $\sigma_{\rm tot} = \max(1.5 \cdot 10^{-4}, \sigma_{\rm eff} + \sigma_{as})$.

5.2 Experiment R0S

Only minor changes as compared to experiment R0V has been introduced in experiment R0S. In (20) and (21) c_a has been changed from $c_a = 4$ in R0V to $c_a = 2$ in R0S, which means a weaker dependence on Ri_b. In (17) the constant 0.01 has been replaced by 0.001 and $\sigma_{\rm bg} = 0$ has been changed to $\sigma_{\rm bg} = 1.8 \cdot 10^{-4} \cdot (\frac{0.1+v}{1+v})$ with the condition $\sigma_{\rm tot} \geq 2 \cdot 10^{-4}\,\mathrm{g\,m^{-3}}$, corresponding to a maximum visibility of 49 km. In (6) $\sigma_{\rm tot} = \max(2 \cdot 10^{-4}, \sigma_{\rm eff} + \sigma_{as} + 1.8 \cdot 10^{-4} \cdot \frac{0.1+v}{1+v})$.

Table 1: Contingency tables of visibility 1510 (12 hour forecasts valid 0 and 12 UTC).

r0V 1510 (80.53 %)							R0V 1510 (77.40 %)						
	[0:1[	[1:5[	[5:10[	[10:20[	[20:]	sum		[0:1[	[1:5[	[5:10[	[10:20[	[20:]	sum
F1	**32**	12	12	12	**10**	78	F1	**18**	7	3	2	0	30
F2	9	**79**	66	43	47	244	F2	7	**1**	6	4	1	19
F3	0	27	**52**	75	86	240	F3	7	9	**10**	3	8	37
F4	3	27	88	**151**	195	464	F4	8	79	78	**59**	52	276
F5	**1**	8	37	116	**281**	443	F5	**5**	57	158	329	**558**	1107
sum	45	153	255	397	619	1469	sum	45	153	255	397	619	1469
%FO	71	52	20	38	45	41	%FO	40	1	4	15	90	44

Table 2: Contingency tables of visibility 1510 (12 hour forecasts valid 0 and 12 UTC).

r0S 1510 (80.53 %)							R0S 1510 (88.84 %)						
	[0:1[	[1:5[	[5:10[	[10:20[	[20:]	sum		[0:1[	[1:5[	[5:10[	[10:20[	[20:]	sum
F1	**32**	12	12	12	**10**	78	F1	**23**	8	8	6	**1**	46
F2	9	**79**	66	43	47	244	F2	17	**50**	38	25	26	156
F3	0	27	**52**	75	86	240	F3	1	80	**108**	99	74	362
F4	3	27	88	**151**	195	464	F4	4	15	97	**234**	398	748
F5	**1**	8	37	116	**281**	443	F5	0	0	4	33	**120**	157
sum	45	153	255	397	619	1469	sum	45	153	255	397	619	1469
%FO	71	52	20	38	45	41	%FO	51	33	42	59	19	36

Table 3: Contingency tables of visibility 1510 (12 hour forecasts valid 0 and 12 UTC).

r0W 1510 (80.33 %)							R0W 1510 (88.56 %)						
	[0:1[	[1:5[	[5:10[	[10:20[	[20:]	sum		[0:1[	[1:5[	[5:10[	[10:20[	[20:]	sum
F1	**33**	13	13	11	**7**	77	F1	**33**	12	11	12	**5**	73
F2	7	**78**	63	44	47	239	F2	6	**43**	26	26	21	122
F3	1	28	**52**	75	91	247	F3	2	82	**90**	65	63	302
F4	3	28	90	**151**	195	467	F4	4	16	120	**246**	341	727
F5	**1**	6	37	116	**279**	439	F5	0	0	8	48	**189**	245
sum	45	153	255	397	619	1469	sum	45	153	255	397	619	1469
%FO	73	51	20	38	45	40	%FO	73	28	35	62	31	41

Table 4: Contingency tables of visibility 1510 (12 hour forecasts valid 0 and 12 UTC).

r0N 1510 (80.53 %)							R0N 1510 (79.44 %)						
	[0:1[	[1:5[	[5:10[	[10:20[	[20:]	sum		[0:1[	[1:5[	[5:10[	[10:20[	[20:]	sum
F1	**32**	12	12	12	**10**	78	F1	**27**	8	5	7	**1**	48
F2	9	**79**	66	43	47	244	F2	9	**13**	11	10	12	55
F3	0	27	**52**	75	86	240	F3	4	15	**15**	10	15	59
F4	3	27	88	**151**	195	464	F4	1	90	98	**85**	80	354
F5	**1**	8	37	116	**281**	443	F5	**4**	27	126	285	**511**	953
sum	45	153	255	397	619	1469	sum	45	153	255	397	619	1469
%FO	71	52	20	38	45	41	%FO	60	8	6	21	83	44

Figure 1: Verification results for October 2015 for 12 h forecasts of visibility (in km) valid at 00 and 12 UTC. Results for OPR are shown in the left column, while the right column shows results from the experiments in Section 5. All contingency tables to the left are identical, representing OPR.

5.3 Experiment R0W

In R0W (11) has been replaced by

$$\widehat{dt} = (sta \cdot f_p + (1 - sta) f_m)(dt + 0.2(1 - r_s) + 0.6(1 - r_2) + 0.2(1 - r_n)), \tag{22}$$

and dt_{land} in (17) has been replaced by

$$dt_{\text{land}} = dt2 + 0.001 \left(1 - \frac{Ri_b}{1 + |Ri_b|}\right) + r_2^{-(3-2/\sqrt{1+v})} - 0.998\, r_2. \tag{23}$$

In (6) σ_{tot} now reads $\sigma_{\text{tot}} = \max(2 \cdot 10^{-4}, \sigma_{\text{eff}} + \sigma_{as} + 1.8 \cdot 10^{-4} \cdot \frac{0.1+v}{1+v})$.

5.4 Experiment R0N

Equation (20) is replaced by $f_p = 1 + (1 + 0.5 Ri_b)^{-1}$ and f_w is calculated as in (14) if $Ri_b > 0$, but is zero if $Ri_b \leq 0$, which means that wind speed has a direct and indirect (through Ri_b) influence on

visibility in stable stratification, but only an indirect effect in unstable stratification. The calculation of dt_{land} is changed to

$$dt_{\text{land}} = dt2 + \left(10^{-3} + \sqrt{\max(5 \cdot 10^{-5}, 1 - r_2)}\right)\left(1 - \frac{Ri_b}{(1 + |Ri_b|)}\right), \tag{24}$$

and σ_{tot} now reads $\sigma_{\text{tot}} = \max(1.2 \cdot 10^{-4}, \sigma_{\text{eff}} + \sigma_{as})$.

6 Verification results

The experiments have been run for October 2015 and the visibility forecasts have been verified against about 24 Danish stations, consisting of a mixture of land and coastal stations. Verification has been done for 12 h forecasts valid 00 and 12 UTC and 18 h forecasts valid 06 and 18 UTC. Results for experiments R0V, R0S, R0W, R0P and R0N are shown as contingency tables in Figure 1 for 12 h forecasts and in Figure 2 for 18 h forecasts. The left columns show verification results for OPR (the operational scheme) and they ought all to be identical. For some unknown reason the results for r0W differs slightly from the others, but is of no concern in the discussion of the experimental results shown in the right columns.

The modifications leading to R0V has a significant impact. The number of forecasts falling below and above the diagonal in the contingency table increases and decreases, respectively, relative to the operational results, shown in the left column. According to Table 1 in Figure 1 and Table 1 in Figure 2 the number of cases with fog (visibility below 1 km) is under predicted and the number of cases with good visibility ($\geq$ 20 km) is over predicted, which is opposite to the operational results. The percentage of 12 h forecasts falling within one class from the observed class (the One Class Error, OCE) has decreased from 80.53 % in VIS (r0V) to 77.48 % in R0V. The corresponding numbers for the 18 h forecasts are 82.77 % and 73.57 %, respectively. The number of extremities (sum of the lower left and upper right 3 numbers) is for the 12 h forecasts 81 in r0V and 73 in R0V, while the corresponding numbers for the 18 h forecasts are 72 and 102, respectively. All these measures indicate that the operational visibility scheme gives a better prediction of visibility than the experimental R0V-scheme, although the lower number of outliers in the 12 h R0V forecasts could indicate a slightly better performance of this version during day. It is believed that the over prediction of good visibility in R0V is mainly due to the assumption of no background contribution to visibility (the latter was replaced by the condition that visibility must not exceed 63 km).

In the next experiment, R0S, a background visibility was therefore reintroduced together with a weaker dependence on Ri_b. The impact was clear, as shown in Figure 1, Table 2 and Figure 2, Table 2. The number of good visibility predictions went from a significant over prediction in R0V to a significant under prediction in R0S. The OCE for the 12 h forecasts increased from 77.40 % in R0V to 85.97 % in R0S and for the 18 h forecasts the increase was from 73.57 % in R0V to 88.84 % in R0S. The extremity numbers also improved, in the 12 h forecasts from 73 to 37 and in the 18 h forecasts from 102 to 44.

In R0W modifications were introduced with the purpose of increasing both the number of fog and good visibility predictions. It can be seen from Table 3 in Figure 1 and Table 3 in Figure 2 that the hit rate for prediction of fog 12 h in advance increased from $51.1\,\%$ in R0S to $73.3\,\%$ in R0W, while the false alarm rate increased from $50.0\,\%$ to $54.8\,\%$. The hit rate for prediction of good visibility increased from $19.4\,\%$ to $30.5\,\%$ and the false alarm rate decreased from $23.6\,\%$ in R0S to $22.9\,\%$ in R0W. In the 18 h forecasts the hit rate for fog increased from $58.2\,\%$ to $70.0\,\%$ and the false alarm rate increased from $50.6\,\%$ in R0S to $58.8\,\%$ in R0W. The number of extremities in the 12 h forecasts increased a bit from 37 to 42 and in the 18 h forecasts more substantially from 44 to 66.

Table 1: Contingency tables of visibility 1510 (18 hour forecasts valid 6 and 18 UTC).

r0V 1510 (82.77 %)							R0V 1510 (73.57 %)						
	[0:1[	[1:5[	[5:10[	[10:20[	[20:]	sum		[0:1[	[1:5[	[5:10[	[10:20[	[20:]	sum
F1	**39**	11	15	9	**7**	81	F1	**22**	4	4	4	**2**	36
F2	20	**92**	57	41	51	261	F2	17	**6**	7	6	7	43
F3	4	79	**99**	108	94	384	F3	8	9	**11**	3	3	34
F4	3	19	69	**186**	312	589	F4	12	114	75	**64**	68	333
F5	**1**	1	8	41	**102**	153	F5	**8**	69	151	308	**486**	1022
sum	67	202	248	385	566	1468	sum	67	202	248	385	566	1468
%FO	58	46	40	48	18	35	%FO	33	3	4	17	86	40

Table 2: Contingency tables of visibility 1510 (18 hour forecasts valid 6 and 18 UTC).

r0S 1510 (82.77 %)							R0S 1510 (85.97 %)						
	[0:1[	[1:5[	[5:10[	[10:20[	[20:]	sum		[0:1[	[1:5[	[5:10[	[10:20[	[20:]	sum
F1	**39**	11	15	9	**7**	81	F1	**39**	9	12	10	**9**	79
F2	20	**92**	57	41	51	261	F2	17	**74**	45	20	22	178
F3	4	79	**99**	108	94	384	F3	8	106	**114**	130	103	461
F4	3	19	69	**186**	312	589	F4	3	13	71	**209**	357	653
F5	**1**	1	8	41	**102**	153	F5	0	0	6	16	**75**	97
sum	67	202	248	385	566	1468	sum	67	202	248	385	566	1468
%FO	58	46	40	48	18	35	%FO	58	37	46	54	13	35

Table 3: Contingency tables of visibility 1510 (18 hour forecasts valid 6 and 18 UTC).

r0W 1510 (83.04 %)							R0W 1510 (84.88 %)						
	[0:1[	[1:5[	[5:10[	[10:20[	[20:]	sum		[0:1[	[1:5[	[5:10[	[10:20[	[20:]	sum
F1	**37**	10	17	9	**6**	79	F1	**47**	18	22	14	**13**	114
F2	22	**92**	52	33	53	252	F2	12	**62**	31	23	36	164
F3	4	79	**103**	114	95	395	F3	5	104	**111**	108	82	410
F4	3	20	69	**189**	313	594	F4	3	18	78	**214**	347	660
F5	**1**	1	7	40	**99**	148	F5	0	0	6	26	**88**	120
sum	67	202	248	385	566	1468	sum	67	202	248	385	566	1468
%FO	55	46	42	49	17	35	%FO	70	31	45	56	16	36

Table 4: Contingency tables of visibility 1510 (18 hour forecasts valid 6 and 18 UTC).

r0N 1510 (82.77 %)							R0N 1510 (78.54 %)						
	[0:1[	[1:5[	[5:10[	[10:20[	[20:]	sum		[0:1[	[1:5[	[5:10[	[10:20[	[20:]	sum
F1	**39**	11	15	9	**7**	81	F1	**40**	11	10	5	**5**	71
F2	20	**92**	57	41	51	261	F2	13	**14**	17	17	17	78
F3	4	79	**99**	108	94	384	F3	6	29	**16**	16	22	89
F4	3	19	69	**186**	312	589	F4	5	128	128	**107**	108	476
F5	**1**	1	8	41	**102**	153	F5	**3**	20	77	240	**414**	754
sum	67	202	248	385	566	1468	sum	67	202	248	385	566	1468
%FO	58	46	40	48	18	35	%FO	60	7	6	28	73	40

Figure 2: Verification results for October 2015 for 18 h forecasts of visibility (in km) valid at 06 and 18 UTC. Results for OPR are shown in the left column, while the right column shows results from the experiments in Section 5. All contingency tables to the left are identical, representing OPR.

The purpose of experiment R0N was (relative to R0W) to reduce the over prediction of fog and at the same time further reduce the under prediction of good visibility. The results for 12 h and 18 h forecasts are shown in Figure 1, Table 4 and Figure 2, Table 4, respectively. It is seen that the over prediction of fog has been reduced to a level where the number of fog predictions almost equals the number of fog observations with a hit rate and false alarm rate for the 12 h forecasts of $60.0\,\%$ and $43.8\,\%$, respectively. The corresponding numbers for the 18 h forecasts were $59.7\,\%$ and $43.7\,\%$. The number of good visibility forecasts increased substantially with a hit rate and false alarm rate for the 12 h forecasts of $82.6\,\%$ and $46.4\,\%$, respectively. The corresponding numbers for the 18 h forecasts were $73.1\,\%$ and $45.1\,\%$. A score S_i is defined by $S_i = 1 - \sqrt{0.5\,((1-h_i)^2 + f_i^2)}$, where h_i is the hit rate for visibility class $i (i = 1 \ldots 5)$ and f_i the corresponding false alarm rate. A perfect forecast ($h_i = 1$ and $f_i = 0$) has $S_i = 1$ and if the forecasts have no hits at all $S_i = 0$. The visibility classes are specified in Figure 1 and 2 (second row from top) with fog as class 1 and good visibility as class 5. Table 2 shows S_i for the experiments described in Section 5. $S_i(0, 12)$ are for the 12 h forecasts

Table 2: Scores for 5 visibility classes (S1 to S5) for 5 different visibility schemes at valid times 00,12 UTC and 06,18 UTC, respectively.

	OPR	R0V	R0S	R0W	R0N
S1(0,12)	0.535	0.490	0.505	0.568	**0.568**
S1(6,18)	0.528	0.452	0.535	0.533	**0.581**
S2(0,12)	**0.414**	0.031	0.325	0.315	0.154
S2(6,18)	**0.404**	0.083	0.393	0.343	0.123
S3(0,12)	0.208	0.147	**0.356**	0.324	0.151
S3(6,18)	0.325	0.170	0.345	**0.354**	0.118
S4(0,12)	0.352	0.208	**0.434**	0.460	0.225
S4(6,18)	0.392	0.181	**0.604**	0.430	0.390
S5(0,12)	0.532	0.642	0.349	0.486	**0.651**
S5(6,18)	0.374	0.616	0.364	0.377	**0.628**
Outliers	153	175	**81**	108	107

valid 0 and 12 UTC and $S_i(6,18)$ are for the 18 h forecasts valid 06 and 18 UTC. The table shows that in terms of number of outliers (last row in the table) R0S performs best, while R0N performs best in terms of scores for the two extreme classes S_1 and S_5.

7 Modifications to the operational visibility scheme: Part 2

In the experiments described above the variation in aerosol content was parameterized very crudely as a function of the wind speed and wind direction of the 10m wind only, in such a way that the maximum aerosol content was obtained when the wind was coming from south and the function gave no contribution when the wind was coming from north exactly (north=0°). Such a parametrization is only valid for regions where non-polluted air is advected by winds from north. This made the scheme non-applicable for most other regions of the world than the danish territory.

7.1 Tropospheric aerosols and their influence on visibility

The effects of atmospheric aerosols is briefly described as these can reduce the visibility significantly. Atmospheric aerosols spans over many particle sizes from approximately $10^{-3}\,\mu\mathrm{m}$ to $10^{2}\,\mu\mathrm{m}$ (the width of a human hair). Aerosols can be divided into different sources, such as biological, solid earth and anthropogenic sources. Biological sources includes pollen, seeds, bacteria, fungi etc. released by plants and animals into the atmosphere. Mechanical action of the wind on the surface are responsible for transporting aerosols, such as dust particles and sea salt, from the Earths surface into the atmosphere.

The global input of particles into the atmosphere from anthropogenic activities is approximately 20 % (Wallace and Hobbs, 2006) which is emitted from highly urbanized areas. The anthropogenic sources are projected to double by the year 2040. The visibility is reduced due to air pollution when the emission rate exceed the rates at which the pollutants are dispersed by the wind. In stable situations pollutants are not as effectively dispersed as in unstable situations and and so the visibility will decrease in stable situations when the amount of pollutants starts to accumulate. A new aerosol content parametrization, described in the next subsection, has been developed to obtain a refined description of the aerosol content.

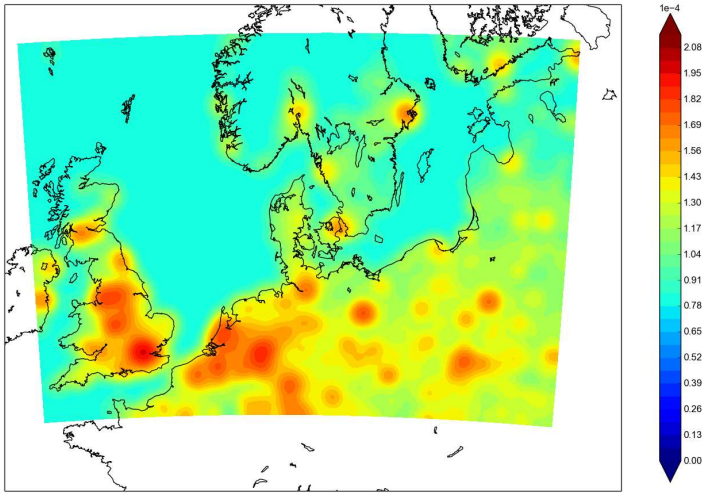

Figure 3: Spatial representation of σ_p.

7.2 Method

Anthropogenic aerosols in urban environments typically reduce visibility by one order of magnitude relative to unpolluted conditions (Jacob, D.J. 1999), and they are therefore an important effect in urbanized areas. The aerosol contribution is based on a global future population density data set (Center for International Earth Science Information Network - CIESIN - Columbia University, and Centro Internacional de Agricultura Tropical - CIAT, 2005). It is argued that highly populated areas are a greater source of aerosols than less populated areas. The population data was interpolated to the model grid (0.03°) by using bicubic interpolation. Population density changes rapidly from highly urbanized areas to areas of very low population. This is especially the case near coastal cities. However, it is not realistic that the polluted air has the same sharp edges as air will be advected downwind and mix with cleaner air. In order to define a realistic background source, the interpolated population data was processed with a 2-dimensional Gaussian filter which works as a smoothing function on the data. The background field, σ_{asb} is defined as

$$\sigma_{asb} = \log\left(1 + \log\left(\frac{1+\sigma_p}{\frac{1}{N}\sum_{i=1}^{N}\sigma_{p,i}} + 1\right)\right) \cdot \sigma_{00} + \sigma_{00}, \tag{25}$$

where σ_p is the population data processed with the Gaussian filter and $\sigma_{00} = 0.8 \cdot 10^{-4}$. σ_p is shown in figure 3.

Notice that all values are above 0. Therefore, also non-polluted areas gives a contribution to the aerosol content. Mechanical action of the wind on the surface emits soil dust, sea salt and debris from vegetation into the atmosphere. These effects are taken in to account in a very crude sense with this method.

The background field is modified to take advection into account as

$$\sigma_{asb}^{\mathrm{mod}} = \sigma_{asb} \cdot \kappa - \vec{v} \cdot \nabla\sigma_{asb}, \tag{26}$$

where the first term of right hand side is a local production term where $\kappa = 0.35$ and the second term on the right hand side is the advection term. The gradient is crudely calculated by separating σ_{asb} into 8 sectors defined by the given wind direction in each grid point (0°,45°,...,315°). By using a characteristic time scale of 1 hour a departure grid point is found. The gradient is calculated by

using the current grid point and the departure grid point. It is a relatively crude way to calculate the gradient. However, more information is needed in order to make a proper trajectory calculation. This makes the scheme unstable for other regions as it works more dynamically compared to the previous scheme.
The aerosol contribution, σ_{ab}, is a function of σ_{asb} and a stability function made such that visibility is decreased in stable situations where less mixing often occurs in the atmospheric boundary layer compared to unstable situations. The reasoning behind this is that pollutants are dispersed with a higher rate in unstable situations. The stability function is defined as

$$f_{as}(Ri_b) = C + a \cdot (1 + b \cdot sta \cdot Ri_b^{-1}), \tag{27}$$

where C, a and b are constants, all with a value of 1. Ri_b is the bulk Richardson number defined in (16) and sta is either equal to 1 or 0 depending on the value of Ri_b. If $Ri_b < 0$, $sta = 0$ and if $Ri_b >= 0$, $sta = 1$. For unstable situations ($Ri_b < 0$), f_{as} is constant with a value of 2. For $Ri_b > 0$, f_{as} decreases with increasing Ri_b. The final aerosol contribution, σ_{ab} is then defined as

$$\sigma_{ab} = \sigma_{asb}^{\mathrm{mod}} \cdot f_{as}^{-1} \cdot S, \tag{28}$$

where $S = 10$ is a scaling factor.

8 Experiments involving population modified aerosols

The experiments described in the present section are all modifications to the visibility scheme R0N, and they all include new definitions of σ_{as} by applying the new aerosol content parametrization outlined in the previous section. Since R0N gave the best verification scores for both fog and good visibility (see Table 2 in Section 6) it was decided to replace the operational scheme OPR (applied as the basis for the experiments in Section 5) with R0N as the basis for the experiments in the present section. This choice was made because the expectation was that introduction of a population dependent aerosol distribution would in most cases contribute to a decrease in visibility and thus move hits in S_5 to lower classes.

8.1 Experiment R0A

The only difference between R0N and R0A is that the aerosol contribution given by (7) is replaced by a population modified aerosol contribution to visibility, $\sigma_{asb}^{\mathrm{mod}}$, given by (26).

8.2 Experiment R0B

In this experiment the population modified aerosol contribution to visibility given by (26) is modified by introducing a dependence on stability through Ri_b. The applied stability function is defined in (27) and the final expression for the contribution from the population modified aerosols is given by (28).

8.3 Experiment R0X

In this experiment everything is the same as in R0B except that the stability functions in (20) and (21) now reads

$$f_p = 0.5 \left(c_n + c_a(1 + Ri_b)^{-1}\right) \tag{29}$$

and

$$f_m = 0.5 \left(c_n + c_a(1 + Ri_b)\right). \tag{30}$$

8.4 Experiment R0Y

This experiment is identical with R0X, except that dt_{land} in (17) has been changed to

$$dt_{\text{land}} = 0.5(dt2 + dtn) + \left(1 - \frac{Ri_b}{1 + |Ri_b|}\right)\left(1 - \frac{q_2}{q_2^*}\right)^2 + 10^{-5}. \tag{31}$$

8.5 Experiment R0Z

This experiment is identical with R0Y, except that dt_{land} in (17) has been changed to

$$dt_{\text{land}} = 0.5(dt2 + dtn) + 10^{-2}\left(1 + \frac{1}{1 + 0.5(dt2 + dtn)}\right), \tag{32}$$

which means that dt_{land} is independent of Ri_b and only depends on the dew point depression at screen level and the lowest model level.

9 Verification results for experiments with population modified aerosols

Verification results for the experiments in Section 8 together with the results for OPR and R0N (presented in Section 6) are shown in Figure 4 for 12 h forecasts valid at 00 and 12 UTC and in Figure 5 for 18 h forecasts valid at 06 and 18 UTC. The population modified aerosol distribution in R0A did, as expected, reduce the number of good visibility (class 5) predictions (from 953 to 897 in the 12 h forecasts and from 754 to 702 in the 18 h forecasts). The reduction of class 5 predictions went mainly to an increase in the number of class 4 predictions (from 354 to 405 in the 12 h forecasts and from 476 to 520 in the 18 h forecasts). Only small changes occurred in the class 1, 2 and 3 predictions. The number of outliers were nearly unchanged (a reduction form 107 in R0N to 104 in R0A).
Introduction of a stability dependence in the population modified aerosol distribution (equation (27) and (28)) in R0B lead to a further decrease in the number of class 5 predictions (from 897 to 529 in the 12 h forecasts and from 702 to 335 in the 18 h forecasts). The reduction in class 5 predictions went mainly to an increase in the number of class 4 (and to a lesser degree also class 3) predictions.
Differences in verification scores between experiments R0Y and R0Z were small. Both had somewhat higher number of predictions for the three lowest classes than R0X. According to Table 3 R0B and R0X had the lowest number of outliers (70 and 71, respectively) and R0X had slightly higher S_1 and S_5 scores than R0B. For S_2 to S_4 the scores were nearly identical in the two versions.
Of all the models R0X had the highest scores for fog (S_1) and the second highest scores for good visibility (S_5). It is a desirable property of a visibility scheme to have high scores for both fog and good visibility. In this respect R0X shows the best performance of all the presented schemes in Section 6 and 8.

In all the visibility experiments discussed in the present report the host model was the DMI-HIRLAM nowcasting model, named RA3. Bias of temperature, specific humidity, cloud water and wind speed in the host model evidently has an impact on the scores obtained by the visibility scheme, regardless of whether the scheme is perfect (which is only hypothetical) or not. The results presented here for October 2015 show that R0X appears to be the best choice with RA3 as the host model, but this may be a wrong conclusion for another host model with a different bias pattern for temperature, specific humidity, cloud water and wind speed. Furthermore the bias pattern may vary seasonally and with prevailing weather type, for example between low and high index NAO (North Atlantic Oscillation). For these reasons there is no guarantee that R0X always will be the optimal choice with RA3 as the host model.

Table 1: Contingency tables of visibility 1510 (12 hour forecasts valid 0 and 12 UTC).

r0N 1510 (80.53 %)							R0N 1510 (79.44 %)						
	[0:1[	[1:5[	[5:10[	[10:20[	[20:]	sum		[0:1[	[1:5[	[5:10[	[10:20[	[20:]	sum
F1	**32**	12	12	12	**10**	78	F1	**27**	8	5	7	**1**	48
F2	9	**79**	66	43	47	244	F2	9	**13**	11	10	12	55
F3	0	27	**52**	75	86	240	F3	4	15	**15**	10	15	59
F4	3	27	88	**151**	195	464	F4	1	90	98	**85**	80	354
F5	**1**	8	37	116	**281**	443	F5	**4**	27	126	285	**511**	953
sum	45	153	255	397	619	1469	sum	45	153	255	397	619	1469
%FO	71	52	20	38	45	41	%FO	60	8	6	21	83	44

Table 2: Contingency tables of visibility for 1510 (12 hour forecasts valid 0 and 12 UTC).

R0A 1510 (80.46 %)							R0B 1510 (85.36 %)						
	[0:1[	[1:5[	[5:10[	[10:20[	[20:]	sum		[0:1[	[1:5[	[5:10[	[10:20[	[20:]	sum
F1	**27**	8	5	7	**1**	48	F1	**27**	8	6	7	**1**	49
F2	9	**14**	11	10	12	56	F2	9	**15**	12	10	13	59
F3	4	15	**17**	10	17	63	F3	4	26	**28**	16	20	94
F4	1	92	112	**97**	103	405	F4	2	98	164	**219**	255	738
F5	**4**	24	110	273	**486**	897	F5	**3**	6	45	145	**330**	529
sum	45	153	255	397	619	1469	sum	45	153	255	397	619	1469
%FO	60	9	7	24	79	44	%FO	60	10	11	55	53	42

Table 3: Contingency tables of visibility for 1510 (12 hour forecasts valid 0 and 12 UTC).

R0X 1510 (85.30 %)							R0Y 1510 (85.50 %)						
	[0:1[	[1:5[	[5:10[	[10:20[	[20:]	sum		[0:1[	[1:5[	[5:10[	[10:20[	[20:]	sum
F1	**30**	8	6	7	**1**	52	F1	**32**	9	8	10	**4**	63
F2	6	**15**	12	11	13	57	F2	4	**18**	15	11	12	60
F3	4	27	**29**	17	21	98	F3	4	37	**33**	26	28	128
F4	2	97	163	**218**	248	728	F4	3	84	157	**215**	255	714
F5	**3**	6	45	144	**336**	534	F5	**2**	5	42	135	**320**	504
sum	45	153	255	397	619	1469	sum	45	153	255	397	619	1469
%FO	67	10	11	55	54	43	%FO	71	12	13	54	52	42

Table 4: Contingency tables of visibility for 1510 (12 hour forecasts valid 0 and 12 UTC).

r0Z 1510 (80.53 %)							R0Z 1510 (85.70 %)						
	[0:1[	[1:5[	[5:10[	[10:20[	[20:]	sum		[0:1[	[1:5[	[5:10[	[10:20[	[20:]	sum
F1	**32**	12	12	12	**10**	78	F1	**32**	9	7	9	**4**	61
F2	9	**79**	66	43	47	244	F2	4	**17**	15	12	11	59
F3	0	27	**52**	75	86	240	F3	4	38	**34**	26	29	131
F4	3	27	88	**151**	195	464	F4	3	84	159	**217**	258	721
F5	**1**	8	37	116	**281**	443	F5	**2**	5	40	133	**317**	497
sum	45	153	255	397	619	1469	sum	45	153	255	397	619	1469
%FO	71	52	20	38	45	41	%FO	71	11	13	55	51	42

Figure 4: Verification results for October 2015 for 12 h forecasts of visibility (in km) valid at 0 and 12 UTC. r0N and r0Z, shown in the left column, are results for OPR, while the other results are from the experiments in Section 8 and experiment R0N from Section 5.

Table 1: Contingency tables of visibility for 1510 (18 hour forecasts valid 6 and 18 UTC).

r0N 1510 (82.77 %)							R0N 1510 (78.54 %)						
	[0:1[	[1:5[	[5:10[	[10:20[	[20:]	sum		[0:1[	[1:5[	[5:10[	[10:20[	[20:]	sum
F1	**39**	11	15	9	**7**	81	F1	**40**	11	10	5	**5**	71
F2	20	**92**	57	41	51	261	F2	13	**14**	17	17	17	78
F3	4	79	**99**	108	94	384	F3	6	29	**16**	16	22	89
F4	3	19	69	**186**	312	589	F4	5	128	128	**107**	108	476
F5	**1**	1	8	41	**102**	153	F5	**3**	20	77	240	**414**	754
sum	67	202	248	385	566	1468	sum	67	202	248	385	566	1468
%FO	58	46	40	48	18	35	%FO	60	7	6	28	73	40

Table 2: Contingency tables of visibility for 1510 (18 hour forecasts valid 6 and 18 UTC).

R0A 1510 (78.88 %)							R0B 1510 (82.22 %)						
	[0:1[	[1:5[	[5:10[	[10:20[	[20:]	sum		[0:1[	[1:5[	[5:10[	[10:20[	[20:]	sum
F1	**40**	11	10	5	**5**	71	F1	**40**	11	10	5	**6**	72
F2	13	**15**	17	17	17	79	F2	13	**16**	19	18	17	83
F3	6	30	**18**	16	26	96	F3	7	43	**26**	21	37	134
F4	6	126	133	**123**	132	520	F4	7	129	171	**230**	307	844
F5	**2**	20	70	224	**386**	702	F5	0	3	22	111	**199**	335
sum	67	202	248	385	566	1468	sum	67	202	248	385	566	1468
%FO	60	7	7	32	68	40	%FO	60	8	10	60	35	35

Table 3: Contingency tables of visibility for 1510 (18 hour forecasts valid 6 and 18 UTC).

R0X 1510 (82.02 %)							R0Y 1510 (83.11 %)						
	[0:1[	[1:5[	[5:10[	[10:20[	[20:]	sum		[0:1[	[1:5[	[5:10[	[10:20[	[20:]	sum
F1	**42**	12	11	5	**7**	77	F1	**46**	15	17	8	**11**	97
F2	11	**15**	18	18	16	78	F2	10	**21**	14	19	17	81
F3	7	44	**26**	22	40	139	F3	4	70	**46**	29	47	196
F4	7	128	171	**235**	304	845	F4	7	93	149	**232**	301	782
F5	0	3	22	105	**199**	329	F5	0	3	22	97	**190**	312
sum	67	202	248	385	566	1468	sum	67	202	248	385	566	1468
%FO	63	7	10	61	35	35	%FO	69	10	19	60	34	36

Table 4: Contingency tables of visibility for 1510 (18 hour forecasts valid 6 and 18 UTC).

r0Z 1510 (82.77 %)							R0Z 1510 (83.24 %)						
	[0:1[	[1:5[	[5:10[	[10:20[	[20:]	sum		[0:1[	[1:5[	[5:10[	[10:20[	[20:]	sum
F1	**39**	11	15	9	**7**	81	F1	**46**	15	16	7	**9**	93
F2	20	**92**	57	41	51	261	F2	10	**20**	15	20	19	84
F3	4	79	**99**	108	94	384	F3	4	70	**46**	29	46	195
F4	3	19	69	**186**	312	589	F4	7	94	150	**234**	305	790
F5	**1**	1	8	41	**102**	153	F5	0	3	21	95	**187**	306
sum	67	202	248	385	566	1468	sum	67	202	248	385	566	1468
%FO	58	46	40	48	18	35	%FO	69	10	19	61	33	36

Figure 5: Verification results for October 2015 for 18 h forecasts of visibility (in km) valid at 6 and 18 UTC. r0N and r0Z, shown in the left column, are results for OPR, while the other results are from the experiments in Section 8 and experiment R0N from Section 5.

Table 3: Scores for 5 visibility classes (S1 to S5) for 7 different visibility schemes at valid times 0,12 UTC and 6,18 UTC, respectively

	OPR	R0N	R0A	R0B	R0X	R0Y	R0Z
S1(0,12)	0.535	0.581	0.581	0.575	**0.621**	0.595	0.606
S1(6,18)	0.528	0.581	0.581	0.577	**0.585**	0.568	0.581
S2(0,12)	**0.414**	0.154	0.166	0.174	0.180	0.205	0.194
S2(6,18)	**0.404**	0.123	0.128	0.135	0.129	0.176	0.166
S3(0,12)	**0.208**	0.151	0.164	0.198	0.198	0.191	0.192
S3(6,18)	**0.325**	0.118	0.127	0.146	0.142	0.212	0.213
S4(0,12)	0.352	0.255	0.240	0.410	0.410	0.408	**0.412**
S4(6,18)	0.392	0.252	0.277	0.413	0.420	0.428	**0.431**
S5(0,12)	0.532	**0.651**	0.644	0.574	0.582	0.574	0.568
S5(6,18)	0.374	**0.628**	0.610	0.458	0.462	0.458	0.452
Outliers	153	107	104	**70**	71	82	79

10 Summary and outlook

For several reasons it is a challenge to predict visibility with high accuracy (see for example Steeneveld et al., 2015). The challenges include

- significant uncertainties in observations/measurements of visibility
- rather crude parametrizations of the direct and indirect (through parametrization of cloud microphysics) effect of aerosols on visibility
- model errors in the input parameters (temperature, specific humidity, cloud water and wind speed) to the visibility scheme
- inaccuracies/errors in the parametrization of visibility
- insufficient vertical and horizontal resolution to properly resolving thin fog layers and local fog patches

Future work on fog prediction at DMI should therefore first of all consider higher vertical (and possible horizontal) model resolution, improvements in the analyses of surface parameters, including soil moisture, in part by expanding the use of data obtained by remote sensing. These improvements should go hand in hand with improvements in the surface scheme applied in the model. A better representation of aerosols and improved parametrization of their direct and indirect effects on visibility is also needed.

In the present report verifications have been done for only one month, which is believed to be a too short period for giving the true picture of the performance of a visibility scheme. The conclusion that R0X appears to have the best verification scores among the evaluated experiments should therefore be considered as preliminary. As a minimum the verifications ought to be done for all seasons, and it should be kept in mind that the verification results depend on both the host model (delivering input parameters) and the applied visibility scheme. This means that improvements in prediction of visibility in general involves both reductions of systematic errors in the host model and improvements of the parametrizations in the visibility scheme.

In a weather prediction model with a vertical and horizontal resolution capable of resolving thin fog layers as well as fog patches at the surface the visibility at screen level could (at least principally) be calculated as a function of precipitation intensity (rain, snow, graupel, hail), cloud water and aerosols at screen level. This would be a simplification in the sense that use of parametrizations involving directly temperature, specific humidity and wind velocity (as is the case for the experiments in the present report) are no longer necessary.

Acknowledgement

The research leading to these results has received funding from the MONALISA 2.0 project of the European Union's Trans-European Transport Network (TEN-T) Programme grant agreement n° [2012-EU-21007-S] and EUCISE2020 project of the the European Union's seventh framework programme under grant agreement n° [608385]

References

[Center for International Earth Science Information Network - CIESIN - Columbia University 2005] Centro Internacional de Agricultura Tropical - CIAT. Gridded Population of the World, Version 3 (GPWv3): Population Density Grid, Future Estimates. Palisades, NY: NASA Socioeconomic Data and Applications Center (SEDAC).

[Cotton, W. R. and R. A. Anthes 1989] Storm and Cloud Dynamics. Academic Press, International Geophysics Series, Vol. 44.

[Jacob, D.J. 1999] Introduction to Atmospheric Chemistry. Princeton University Press, 1999. pp. 114-148.

[Kunkel 1984] Parameterization of droplet terminal velocity and extinction coefficient in fog models. J. Climate Appl. Meteor., 23, 34-41.

[Petersen, C. and N.W. Nielsen 2000] Diagnosis of visibility in DMI-HIRLAM. DMI Scientific Report 00-11.

[Steeneveld, G.J., R.J. Ronda and A.A.M. Holtslag 2015] The challenge of forecasting the onset and development of radiation fog using mesoscale atmospheric models. Boundary-Layer-Meteorol, 2015,154,265-289.

[Wallace, J.M. and Hobbs, P.V. 2006] Atmospheric Science, 2nd Edition. Elsevier 2006. pp. 170-175.

11 Previous reports

Previous reports from the Danish Meteorological Institute can be found at:
http://www.dmi.dk/en/learn/